RINOPOLYCRETE - TOWARDS A CEMENT-FREE AND FULLY RECYCLED CONCRETE

PROJECTO FCT
PTDC/ECI-COM/29196/2017

Recycled inorganic polymer concrete - Towards a cement-free and fully recycled concrete

(RInoPolyCrete)

Task 3 - Report 4

Results and discussion of the experimental investigation on binary mixes containing alkali-activated municipal incinerator bottom ashes and fly ash

TABLE OF CONTENTS

LIST OF FIGURES

LIST OF TABLES

ACRONYMS

AAM	Alkali-activated materials
Al	Aluminium
C-(N-)A-S-H	Calcium (alkali) aluminosilicate hydrate gel
EDS	Energy dispersive X-Ray spectroscopy
FA	Fly ash
ICP-OES	Inductively coupled plasma - optical emission spectrometry
MIBA	Municipal solid waste incinerator bottom ash
MSW	Municipal solid waste
Na_2SiO_3	Sodium silicate
NaOH	Sodium hydroxide
N-A-S-H	Sodium aluminosilicate hydrate gel
pH	Hydrogen potential
XRD	X-ray diffraction
XRF	X-ray fluorescence

1 Introduction

In 2018, the generation of municipal solid waste (MSW) in the EU increased by 2.5% compared to 2016. For the year 2020, this value is expected to be significantly higher, since variables such as working from home due to the pandemic, which had an increase of 6.9% in the 27 EU State Members in 2020 when compared to 2019 (from 5.5% to 12.4%) [1], could imply a greater amount of waste generated and disposed.

This upward trend in the amount of generated MSW, also directly associated with population growth [2], adds value to the research on the technical feasibility processed waste streams generated from the combustion of solid waste, valuable for the scientific community.

Municipal solid waste incinerator bottom ash (MIBA) has been studied as a precursor of alkaline activated materials (AAM), revealing two major weaknesses:

    i. Presence of metallic aluminium that reacts in an alkaline solution to produce hydrogen gas, which was widely analysed and discussed in Report 2.3;

    ii. Low content of amorphous aluminosilicates.

In Report 2.4, it was determined that the optimal ratio, at 28 days of curing of $Na_2O/Binder$ and SiO_2/Na_2O for FA and MIBA corresponded to 15/1.0 and 8/0 respectively, and the compressive strength developed by the mortars with FA was around 10 times greater than that obtained with MIBA (50.7 MPa vs. 5.47 MPa).

In order to obtain an AAM with better mechanical properties, yet with the highest possible MIBA content, replacements of FA with MIBA of 0%, 25%, 50%, 75% and 100% were made. Two alkaline activator designs were also proposed: optimal alkaline activator (OAA) and constant alkaline activator (CAA). Mortar mixes were then produced and subjected to characterization. In the fresh state, consistence [3] and density [4] were evaluated, whereas, in the hardened state, compressive and flexural strength [5], dry bulk density [6] and dynamic modulus of elasticity [7] were determined at 7, 28, 91 and 182 days of age. In addition, shrinkage [8], water absorption by capillarity [9], water absorption by immersion [10] and carbonation depth [11] were evaluated in the hardened state for the mixes made with the CAA design.

2 Materials and methods

The methodology, materials, mixing process and test methods were already described in Report 3.2. Nonetheless, additional information about the methodology carried out is presented in Figure 1, which corresponds to an adaptation of the conceptual model of "geopolymerization" presented by Duxson et al. [12]. In the model elaborated by these authors, although the steps required for the processing of the raw materials are not included, in the adaptation made herein, the MIBA pre-treatment (explained in detail in subchapter 3.2) was included as preliminary step. This step is followed by the addition of the second precursor, which corresponds to type F FA. The other conceptual stages can be reviewed in detail in the cited reference.

Even though most of the experimental campaign has been described in Report 3.2, additional relevant aspects were added to section 2.1 in this report, describing the two designs established for the alkaline activator.

2.1 Alkaline activator design

The first design of the alkaline activator, named optimal alkaline activator (OAA), was established from the optimal ratio found in Report 2.4, based on the proportionality of each precursor. Therefore, for the mix with 0% MIBA (0M) the values for the Na_2O/Binder and SiO_2/Na_2O ratios were 15% and 1 (15/1) respectively, and for the mix with 100% MIBA (1M) they were 8% and 0 (8/0). For 25% MIBA (0.25M), the ratio used was 13.25/0.75; for 50% MIBA (0.5M) it was 11.5/0.5 and for 75% MIBA (0.75M) it was 9.75/0.25.

The second design of the alkaline activator, named constant alkaline activator (CAA), consisted in defining the average ratio of 11.5/0.5 for all proportions of precursors. Figure 2 summarizes the aforementioned.
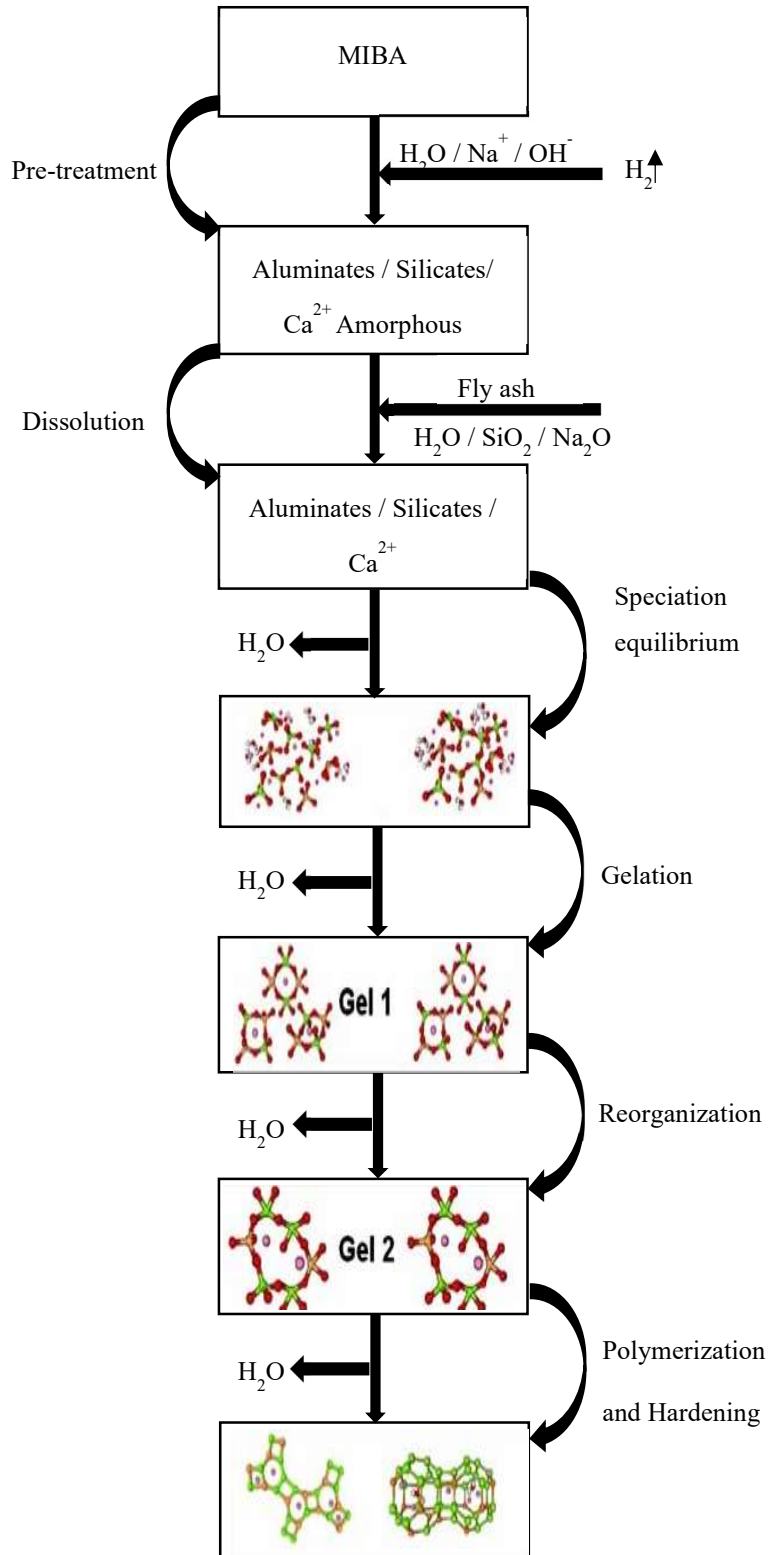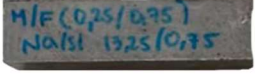
Figure 1 - Adaptation of the conceptual model of geopolymerization by Duxson et al. [12]

SI/NA$_2$O	NA$_2$O/BINDER	MIBA QUANTITY		SI/NA$_2$O	NA$_2$O/BINDER	MIBA QUANTITY	
0.5	11.5			0	8		
		1				1	
0.5	11.5			0.25	9,75		
		0.75				0.75	
0.5	11.5			0.5	11.5		
		0.5				0.5	
0.5	11.5			0.75	13.25		
		0.25				0.25	
0.5	11.5			1	15		
		0				0	

Figure 2 - Alkaline activator designs

3 Results and discussion

3.1 Characterization of the waste precursors

3.1.1 X-ray fluorescence

Table 1 shows the chemical composition of the MIBA (produced in January 2019) and of the FA used in the present investigation. The data show that the sum of the oxides $SiO_2 + Al_2O_3 + Fe_2O_3$ corresponds to 88.7% and 64.3% for FA and MIBA, respectively. When comparing these values with those of ASTM C618-5 [13], it is possible to classify FA as type F, in which the sum of the oxides has a minimum established value of 70%. In the case of MIBA, the classification as per ASTM indicates that the waste can be classified as type C fly ash, since the value exceeds the established limit of 50% for the sum of the oxides. According to the

literature, 66% of MIBAs comply with this limit [14].

Table 1 - Chemical composition of raw materials, FA and MIBA (% by mass)

Materials	FA (%)	MIBA (%)
Al_2O_3	25.5	8.82
CaO	2.28	18.3
Fe_2O_3	6.90	6.68
K_2O	2.74	1.59
MgO	1.83	4.00
Na_2O	1.29	6.53
SiO_2	56.3	48.8
SO_3	0.80	1.36
Cl^-	0.0	0.0

Figure 3 shows the ternary diagram SiO_2 - Al_2O_3 - CaO, which corresponds to the main oxides directly responsible for the generation of oligomers that give rise to the N-A-S-H or C-(N-)A-S-H products, once they are dissolved in alkaline environments.
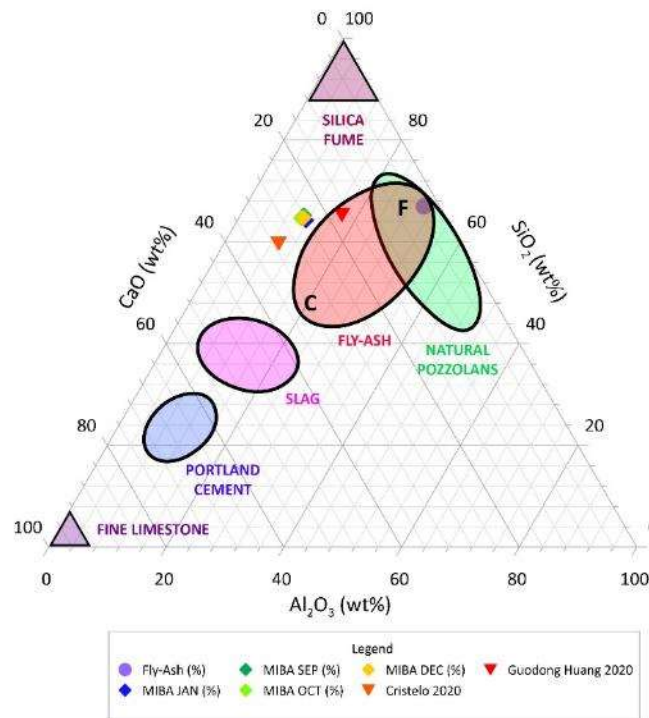
Figure 3 - Ternary diagram of CaO-Al_2O_3-SiO_2 content [15]

It can be observed that the MIBA samples made in September 2018, October 2018, December 2018 and January 2019 are similar to each other and to samples from other studies [16, 17]. Finally, Figure 3 shows the typical areas for each pozzolanic addition [15], confirming the previously established classification for the waste of the present study.

3.1.2 X-ray diffraction

Figure 4 corresponds to the X-ray diffraction (XRD) results of the MIBA samples used in the present study. The crystalline phases observed are quartz (SiO_2), calcite ($CaCO_3$), magnetite ($Fe^{2+}Fe^{3+}2O_4$), fayalite ((Fe^{2+})$_2SiO_4$), magnesian ($MgCO_3$), microcline ($KAlSi_3O_8$), magnesium phosphate ($Mg_3(PO_4)_2$), sodium calcium iron phosphate and anhydrite ($CaSO_4$). These results are consistent with those of other research works where similar minerals were found for MIBA [18, 19].

Figure 5 corresponds to the XRD results obtained for the FA sample used. The crystalline phases observed are quartz (SiO_2), lime (CaO), maghemite ($Fe^{3+}2O_3$) and mullite. The mineralogical characterization of FA is similar to that reported by other authors [20, 21].

3.1.3 pH

The hydrogen potential test was carried out using a digital pH meter from HACH. The procedure for pH determination was based on ASTM D4972 [22]. MIBA and FA presented values of 9.50 and 10.70, respectively, which indicates the alkaline nature of both precursors. High pH values are key in the alkaline activation process.
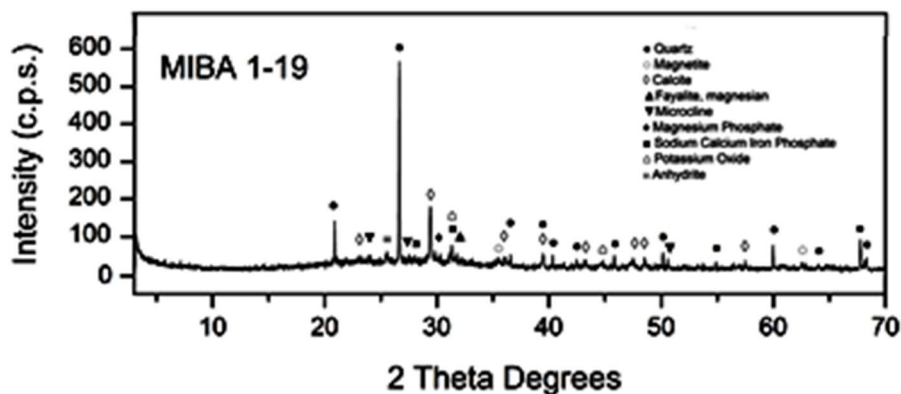
Figure 4 - XRD pattern of MIBA
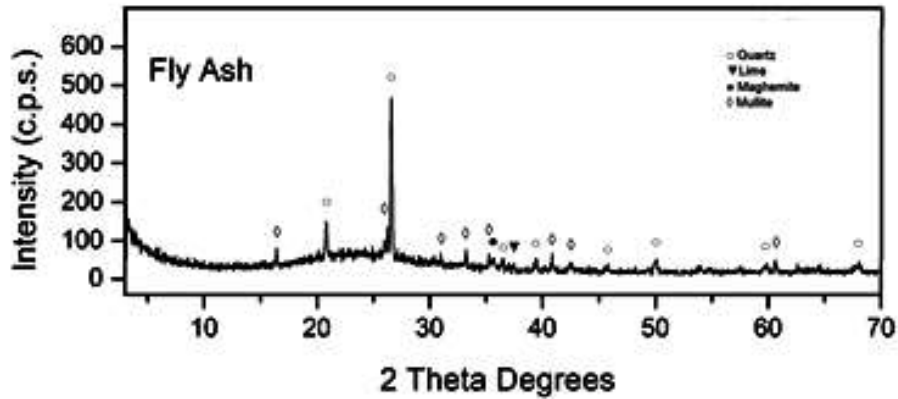
Figure 5 - XRD pattern of FA

3.1.4 Quantification of metallic aluminium in MIBA

The chemical reaction to produce gaseous hydrogen from metallic aluminium and sodium hydroxide corresponds to equation 1A. Stoichiometric quantities (atomic and molecular weights in grams) are presented in equation 1B.

$$2Al^0 \ + \ 2NaOH \ + \ 6H_2O \ \rightarrow \ 2NaAl(OH)_4 \ + \ 3\,H_2 \uparrow \qquad \text{Eq. 1A}$$

$$54g \ + \ 80g \ \ + 108\,g \ \ \rightarrow \ \ 236g \ \ \ + \ 6g \uparrow \qquad \text{Eq. 1B}$$
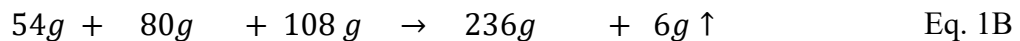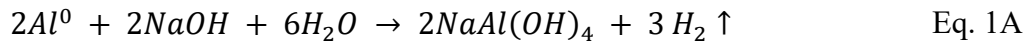
From the stoichiometric quantities, it was determined that 0.11 g of $H_2\uparrow$ were produced per gram of aluminium consumed (Eq. 2).

$$g\,H_2 \uparrow= 1 \text{ g Al}° \text{ x } \frac{6\,g\,H_2 \uparrow}{54\,g\,Al°} = 0.11\,g \qquad \text{Eq. 2}$$

From the reaction of 0.1 g of metallic aluminium with a 2.5 M NaOH solution (excess reagent), the volume of water displaced by the hydrogen gas produced was measured experimentally in an inverted test tube, which was connected through a glass tube to a three-nozzle balloon (Figure 6a). The theoretical value from Eq. 1A corresponds to 143.03 ml of H_2 gas.

Three trials were carried out to determine the average experimental value and calculate the error in function of the theoretical one. The temperature at which the reaction was carried out

was 43 °C. This heat was due to the exothermic reaction of NaOH in water.

The density of the hydrogen at 43 °C and 1 atm. of pressure is 0.0766 kg/m^3 [23]. From this property and the mass of hydrogen produced by each gram of aluminium (Eq. 3), it was possible to determine the theoretical volume of hydrogen generated.

$$v = \frac{m}{\rho}; \quad v_{H_2} = \frac{0,11\ g}{0.0000766\ g/ml} = 1436.03\ ml \qquad \text{Eq. 3}$$

One gram of metallic aluminium generates 1.436 litres of H$_2$. Table 2 shows the measurements made in triplicate for 0.1 g of pure metallic aluminium.

Table 2 - H$_2$ release by 0.1 Al°

Vi (ml)	Vf (ml)	Vexp (ml)
10	142	132
30	156	126
28	164	136
Average		131.33
Std.Dev.		5.03
Error		8%

To quantify the metallic aluminium in MIBA, the test was carried out with 30 g of this precursor and 800 ml of a 2.5 M NaOH solution. The results are presented in Table 3.

Table 3 - H$_2$ release by 30 g of MIBA

Vi (ml)	Vf (ml)	V exp (ml)
50	218	168
41	200	159
23	172	149
Average		158.67
Std.Dev.		9.50

Using the density, the milligrams of hydrogen present in 158.7 ml of the gas were determined as follows (Eq. 4):

$$v \times \rho = m; \quad 158.67ml \times 0,0000766\frac{g}{ml} = 0.01215\ g = 12.15\ mg \qquad \text{Eq. 4}$$

Where v corresponds to the volume in ml, ρ is the density in g/ml and m, the mass in mg. Using the stoichiometries weights, in Eq. 5, the amount of metallic aluminium that produces this quantity of hydrogen is determined.

$$g\ Al° = 0.01215\ g\ H_2 \uparrow \ \text{x}\ \frac{54\ g\ Al°}{6\ g\ H_2 \uparrow} = 0.1640\ g\ Al°$$

Eq. 5

Therefore, in 30 g of MIBA there are ~164 mg of metallic aluminium, and it can be concluded that there are 5.46 g of Al/kg of MIBA and that this aluminium in contact with an excess NaOH solution produces 7.91 L of $H_2 \uparrow$/kg of MIBA. Figure 6b shows the relationship between the hydrogen released by MIBA and time in minutes.
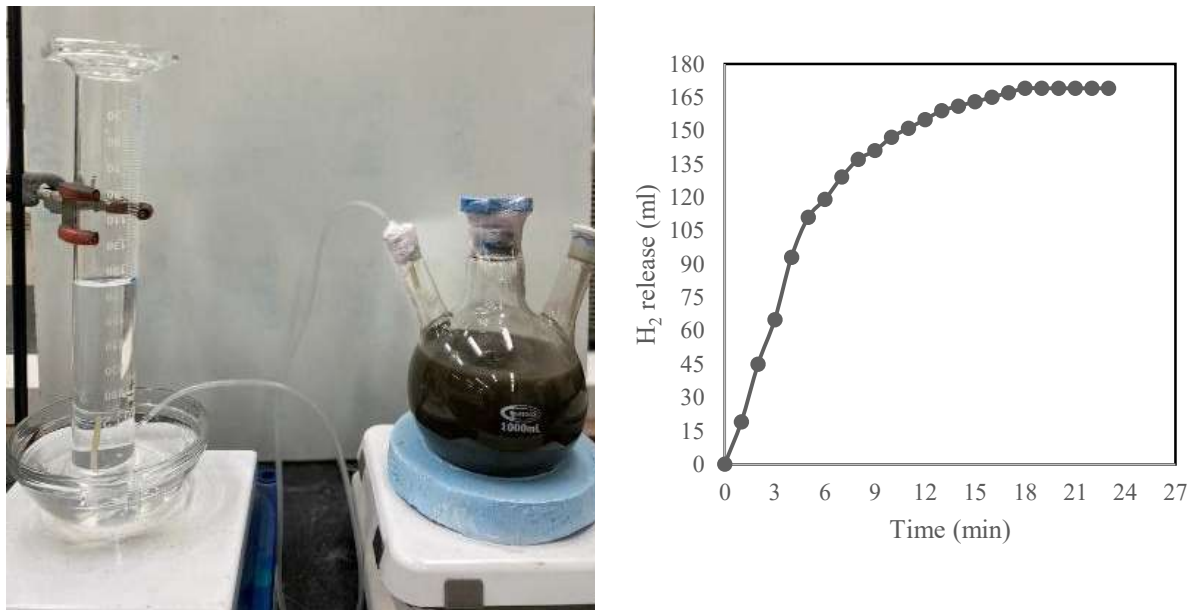
Figure 6 - Quantification of metallic aluminium in MIBA: (a) experimental setup (b) H_2 released by MIBA over time

3.1.5 Pozzolanic activity index

In the modified Chappelle test determined by titration with 0.1 M HCl, the content of CaO consumed by the reactive phases present in FA were determined during 16 h of reaction at $90 \pm 5\ °C$ of 2 g CaO grade laboratory and 1 g of the by-product diluted in decarbonated water.

The reactions presented in the titration are the following (Eqs. 6 and 7):

$$CaO + 2HCl \rightarrow CaCl_2 + H_2O \qquad \text{Eq. 6}$$

$$Ca(OH)_2 + 2HCl \rightarrow CaCl_2 + 2H_2 \qquad \text{Eq. 7}$$
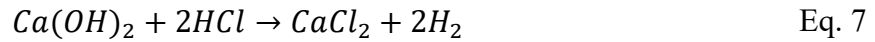
Therefore, it is possible to calculate the mg CaO / g of by-product [24] (Eq. 8):

$$\frac{mg\ CaO}{g\ by - product} = \frac{28\ x\ (v_3 \times m_3 - v_2) \times F_c \times 2 \times 2}{m_4 \times m_3 \times m_2}\ x\ 1.32 \qquad \text{Eq. 8}$$

Where m_2 is the mass of the pozzolanic material expressed in grams, m_3 is the mass of CaO mixed with pozzolanic material, m_4 is the mass of CaO in the blank test, v_2 is the HCl consumed by the sample (ml); v_3 is HCl consumed by the blank (ml); F_c, the correction factor for a 0.1 M solution of HCl.

Through the Chappelle test, a value of 1513 mg of CaO per g of FA was obtained, which is higher than the minimum limit, 330 mg CaO/g of addition established by Raverdy et al. [25, 26]. Nevertheless, it should be noted that, according to the standard NBR 15895 [24], the Chappelle test is not recommended for samples with high Ca content. Evaluating the amorphous aluminosilicates phases in MIBA should be made by means of inductively coupled plasma optical emission spectrometry (ICP - OES) [27, 28].

3.2 MIBA pre-treatment

In order to avoid the production of H_2 in AAM mixes, it was established that a pre-treatment of MIBA was required. In this treatment, the NaOH concentration varied depending on the alkaline activator for a fixed reaction time of 24 hours. The main reaction that takes place in the pre-treatment is the following (Eq. 9):

$$2Al\ +\ 2NaOH\ +\ 6H_2O\ \rightarrow\ 2NaAl(OH)_4\ +\ 3\ H_2 \uparrow \qquad \text{Eq. 9}$$
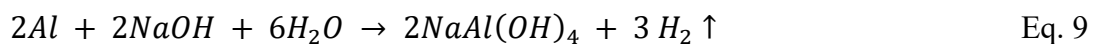
In this reaction, ~5.46 grams of aluminium are oxidized for each kg of MIBA by an exothermic oxidation reaction (-16.3 kJ/g Al°).

In the present research, the heat released in the reaction of dissolving NaOH in water was used as catalyst for the release of hydrogen (46.2 kJ/mol at a NaOH concentration of 1 mol/L). At a higher concentration of alkali, the reaction of metallic aluminium will be favoured due to increased heat input [29]. Rosenband and Gany [30] studied the behaviour of the release of hydrogen associated with the reaction of aluminium with water at various temperatures, confirming that, when the water reached 74 °C, the reaction occurred in a shorter time than when they used water at 50 °C. In the present work, the reaction temperature of the NaOH solution used to treat MIBA was between 80 °C and 83 °C.

NaOH suffers a complete dissolution in water and, therefore, the concentration of the solute will be equal to the concentration of the ions in the aqueous medium (Eq. 10):

$$NaOH \rightarrow Na^+ + OH^-$$
Eq. 10

The concentration of NaOH was determined experimentally through the titration of the alkaline solution with hydrochloric acid (HCl) and using phenolphthalein as an indicator. The chemical reaction that takes place is as follows (Eq. 11):

$$NaOH + HCl \rightarrow NaCl + H_2O$$
Eq. 11

The experimental molarity of the base was determined through the following formula (Eq. 12):

$$M_{NaOH} = \frac{V_{HCl} \times M_{HCl} \times \#H^+_{given}}{V_{NaOH}}$$
Eq. 12

Where M_{NaOH} is molarity of sodium hydroxide, V_{NaOH} is the volume of sodium hydroxide solution in titration (50 ml), M_{HCl} is the molarity of hydrochloric acid (2 M), V_{HCl} is the consumed volume of hydrochloric acid solution and $\#H^+_{given}$ is the number of hydronium ions released in the acid-base neutralization reaction.

In the pre-treatment, MIBA was mixed with a solution containing the amount of NaOH needed for each mix. After this stage, FA and Na_2SiO_3 were added to the rest of the materials to produce the AAM mixes.

In the case of the OAA design, the concentration of the hydroxyl ion increases when the MIBA content in the mixes decreases (Figure 7a). Hence, the elimination of aluminium in the mixes with a lower content of this precursor will be more efficient.

However, for the CAA design, the OH^- concentration in the pre-treatment stage was the same for all mixes: 8.37 M (Figure 7b). With increasing ratio between the sodium hydroxide solution and the MIBA mass, it is expected that the oxidation reaction of metallic aluminium will be more efficient in the mixes with lower MIBA content.

(a)   (b)
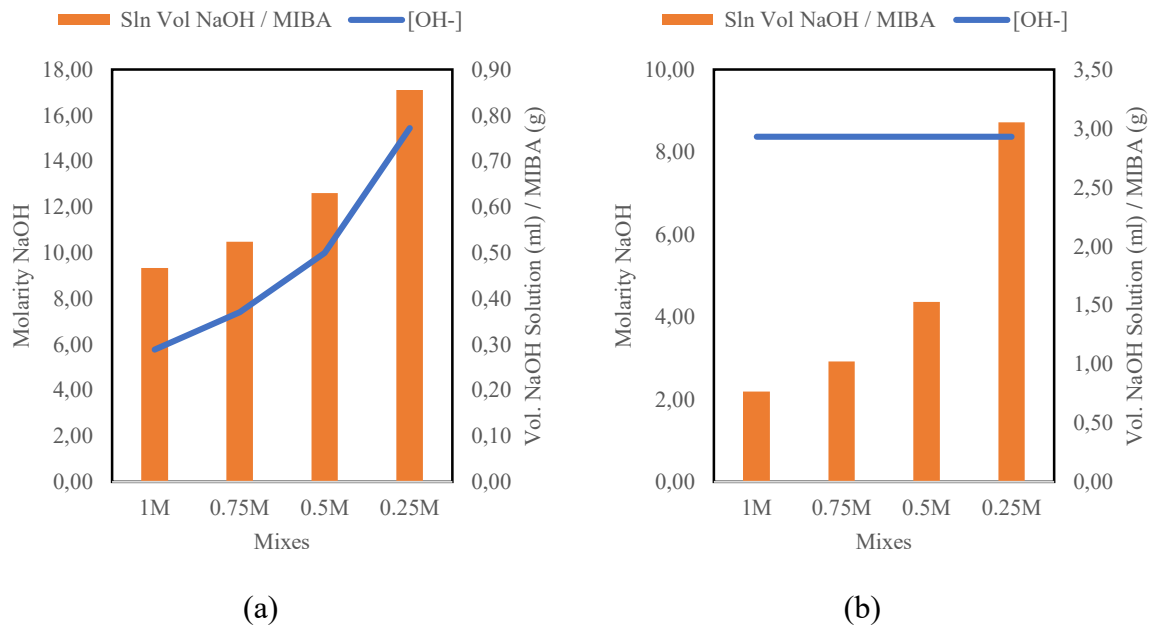
Figure 7 - Concentration and volume of the alkaline solution in the MIBA pre-treatment:
(a) OAA design and (b) CAA design

3.3   Fresh-state properties

3.3.1   Consistence

The workability of the mixes was evaluated based on the consistence by the flow table test described in EN 1015-3 [3]. The flow values determined for the mixes in the fresh state with OAA and CAA are presented in Figure 8a and Figure 9b, respectively. According to the results obtained, an increase of 54% in flow values was found for the 1.0M mix with CAA when compared to that of the same mix with OAA. In the same way, for the mix 0.75M, an increase

of 39% was observed, whereas for the mix 0.25M that increase was of 4%. CAA design provided that all the mixes were in a plastic and fluid state, contrary to what was obtained with the OAA design. It is evident in both figures that the factor with the greatest influence on workability is the FA content. As this content increased, the fluidity of the mix also increased.
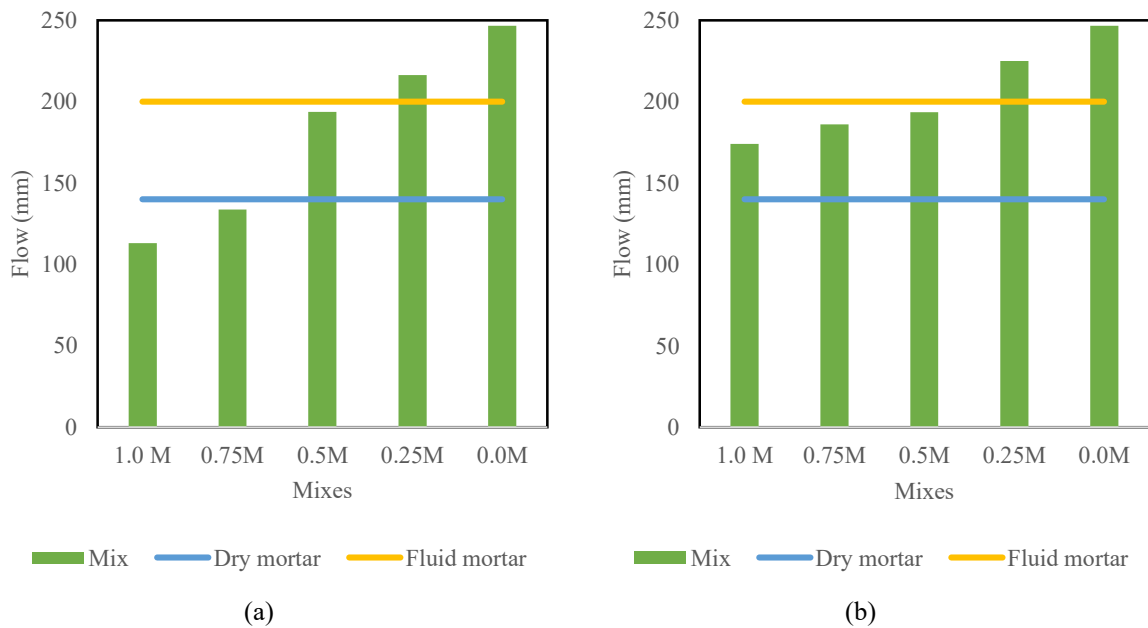
Figure 10 - Flow values of: (a) OAA mixes and (b) CAA mixes

The results reported in this report are in accordance with other studies. Among them, Das et al. [31] determined the workability of alkali-activated concrete mixes using type F FA as precursor, incorporating low amounts of lime and silica lime as replacement of the FA, and having as alkaline activator NaOH and Na_2SiO_3. The cited work reported a decrease in slump when the replacement ratio of FA increased (about 60 mm for 5% FA replacement and of 15 mm for 10% FA replacement). Other authors such as Kuri, Khan and Sarker [32] concluded that when increasing the amount of magnesium ferronickel, along with a decrease in the amount of type F FA in alkali-activated pastes, the fluidity decreased. Indeed, the high workability granted by fly ash can be ascribed to the spherical morphology of its particles, which acts to reduce the viscosity of the fresh material by reducing interparticle friction [33].

3.3.2 Density

The determination of bulk density in the fresh state was carried out according to EN 1015-6 [4], whereas that property in the hardened state was determined according to EN 1015-10 [6]. Figure 11a and Figure 11b show the density in the fresh state and in the hardened state at 28 days of the mixes made with the OAA and the CAA design, respectively. For the mixes with the OAA design (Figure 11a), density in the fresh state presented values between 1.90 and 2.27 g/cm^3 with a mean value of 2.09 g/cm^3. In turn, for the mixes with the constant alkaline activator design (Figure 11b), the density of the mortars in the fresh state increased as the MIBA content decreased, a behaviour similar to that presented in the hardened state.

(a)	(b)
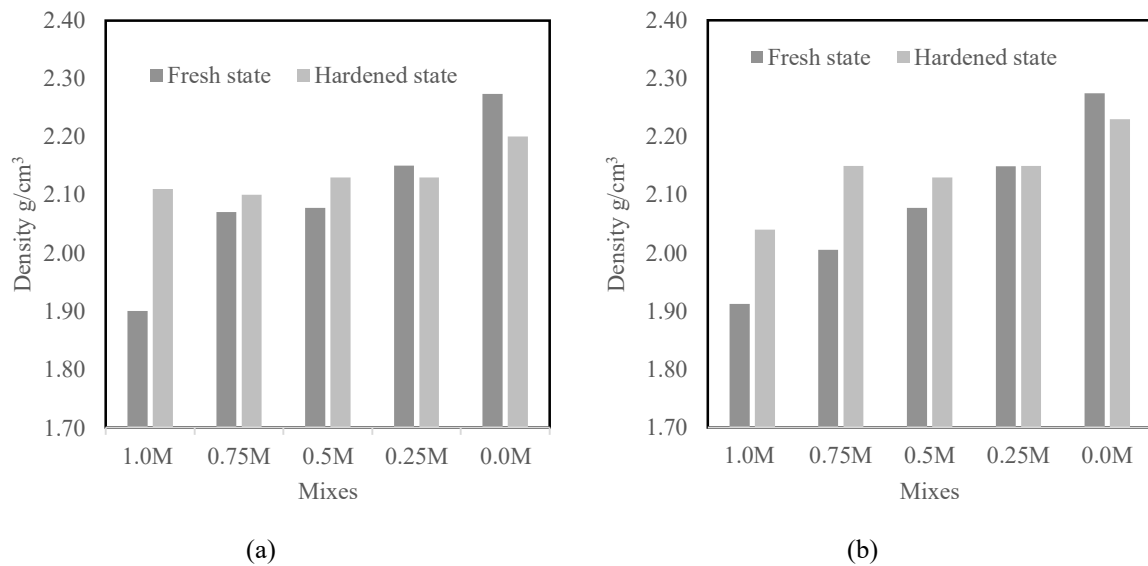
Figure 11 - Fresh and hardened state densities of: (a) OAA mixes and (b) CAA mixes

The mixes with higher FA contents, by showing greater densities in the hardened state, will probably also present better mechanical properties, as they are more compact. On the other hand, the mixes with higher MIBA contents tend to present lower densities, which can be attributed to residual aluminium that, when in contact with Na_2SiO_3, releases H_2 gas, leading to the foaming of the mortar [34].

3.4 Hardened-state performance

3.4.1 Compressive strength

Figure 12 shows the results of compressive strength at 7, 28, 91 and 182 days for the OAA and CAA mixes. The maximum 28-day compressive strength belonged to the 100% FA mix: 61 MPa and 38.63 MPa for the OAA and CAA designs, respectively. The minimum values occurred in the mix with 100% MIBA; 5.36 MPa and 5.72 MPa for the OAA and CAA designs, respectively. The 28-day and 182-day compressive strength values of the mixes with 50/50 of MIBA/FA were of 19.8 MPa and 25.2 MPa, respectively. Marginal strength increase was observed in OAA mixes containing 25% FA in comparison with those without it (i.e. ~100% increase after 28 days).
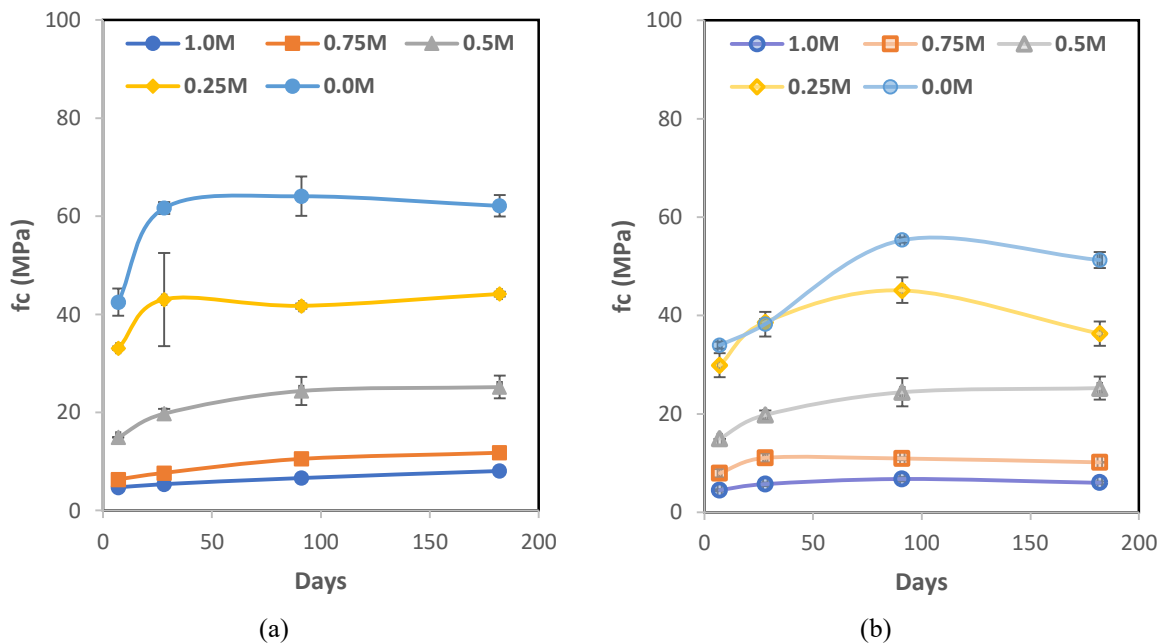
Figure 12 - Compressive strength of: (a) OAA mortars and (b) CAA mortars

For longer curing times, the trend maintained regarding the mixes with the highest and lowest compressive strengths. This clearly indicates that there is an enhanced strength development with increasing FA content.

The crosslinking of the reaction product in the activation process of type F FA (a precursor characterized by having a high content of Al and Si and a low content of Ca) is analysed as a monolithic alkali-activated gel, which is not yet completely understood [35], while MIBA is

more similar to a precursor with a high Ca content, where the main reaction products correspond to C-A-S-H gel and its structure is strongly associated with the activator used [36]; the type of gel that is formed when mixing FA and MIBA-like precursors will depend on the reaction mechanisms, which will be analysed in subsequent studies.

By mixing the two materials to obtain an AAM, the FA structure can function as a net that binds MIBA particles with low pozzolanicity. This means that MIBA does not completely deteriorate the mechanical properties of the new material, but reduces them proportionally to the percentage of addition.

Wongsa et al. [37] studied mixes where type C FA was replaced with MIBA at 0%, 20%, 40% and 100%. These authors then concluded that the 20% and 40% replacement levels of FA with MIBA led to the highest compressive strengths (respectively, 53 MPa and 45.6 MPa when compared with 42 MPa of the mix without MIBA) and 100% to the lowest (10.6 MPa). The improved performance when adding MIBA may have been partly due to the greater presence of glass particles, which are known to contribute actively to the strength development of alkali-activated mixes.

In another research, Kuri et al. [32] studied binary mixes, where type F FA was replaced at 0%, 25%, 50%, 75% and 100% with ferronickel magnesium slag. The alkaline activator used was a mix of NaOH and Na_2SiO_3 and two curing conditions were used: thermal curing at 60 °C for 24 h and ambient curing. With thermal curing, when the content of ferronickel increased from 0% to 75%, the compressive strength increased from 33 MPa to 45 MPa at 28 days of curing. However, for the AAM with 100% ferronickel slag, the compressive strength was substantially reduced to 16 MPa. The interesting thing about this research is that the morphology presented by ferronickel is similar to that presented by MIBA, with both residues being very well coupled in the formation of a new material.

Hosseini et al. [38] evaluated binary alkali-activated mixes with sub-bituminous coal fly ash (type C) and bottom ash (BA) from the same coal power plant. FA and BA had a CaO content of 12.85% and 12.45%, respectively. They found that, since FA is the most reactive component, it leads to a more compact structure (translated into higher density) and, thus, to higher compressive strength.

Compressive strength was also determined for carbonated mortars made with the CAA design. To this end, 28 days after the sealed curing, the prismatic specimens were cured in a carbonation chamber with 5% CO_2 for 7, 14 and 28 days and their compressive strength determined at 35, 49 and 77 days, respectively, after their production.

Figure 13 shows that the compressive strength of carbonated mortars was substantially higher than that of uncarbonated mortars.

Figure 13 - Variation in compressive strength values between uncarbonated and carbonated mortars with CAA design

For instance, 28 days after the carbonation curing, the compressive strength for the 1.0M mix was 19.12 MPa, around 240% higher than the maximum value reported for the uncarbonated mix (8.08 MPa). For the 0.5M mix, after 28 days of carbonation, the compressive strength was around 40% higher than the maximum value reported for the uncarbonated mix. In addition, for the 0.0M mix, 28 days of carbonation led to a compressive strength increase of 30%. From the results obtained, it can be concluded that the highest relative increase in compressive strength due to carbonation occurs for the mixes with the highest proportions of MIBA, as it is a precursor with relatively high calcium content. This behaviour is associated with the precipitation of calcium carbonate ($CaCO_3$) in the capillary pores of the AAM matrix, which causes an increase in densification, in cohesion and thus in compressive strength [39]. In the

mix with 100% FA, which is classified as type F, the formation of this product occurs but to a lesser extent due to the lower presence of Ca-bearing phases. However, a notable increase was nevertheless observed inferring the existence of another strength enhancing mechanism; it is likely related to the carbonation of Na^+ ions, leading to the formation of sodium carbonates as well as the greater polymerization of existing silica gels resultant from N-A-S-H phases.

Regarding carbonation depth, the phenolphthalein indicator test did not present any coloration, indicating that the matrix had a pH lower than 9 and thus presenting "complete carbonation" after 28 days in the carbonation chamber. Consequently, despite carbonation leading to an improvement in compressive strength, it is detrimental to AAM if applied in steel-reinforced structures [40].

3.4.2 Flexural strength

Figure 14 shows the results of flexural strength at 7, 28, 91 and 182 days for the mixes made with OAA and the CAA designs. As found for compressive strength, the maximum flexural strengths were obtained for the mix with 100% FA and the minimum values for the mix with 100% MIBA, a trend that is maintained for longer curing times. By mixing the two materials to obtain an AAM, the FA structure can function as a net that binds MIBA particles with low pozzolanicity. This means that MIBA does not completely deteriorate the flexural strength of the new material, but reduces them proportionally to the percentage of addition.

The behaviour obtained in terms of this mechanical property is explained in similar way that for compressive strength, which was already described in section 3.4.1.

Figure 15 shows that the flexural strength of carbonated mortars was substantially higher than that of uncarbonated mortars. For instan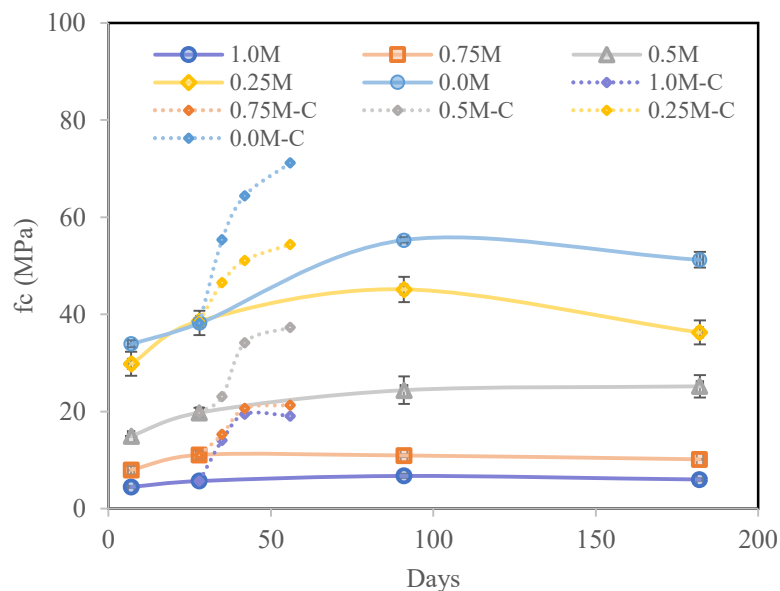ce, 28 days after the carbonation curing, the flexural strength for the 1.0M mix was 4.50 MPa, around 285% higher than the maximum value reported for the uncarbonated mix (1.58 MPa). For the 0.5M mix, after 28 days of carbonation, the flexural strength was around 28% higher than the maximum value reported for the uncarbonated mix. In addition, for the 0.0M mix, after 28 days of carbonation, the flexural strength was similar to the maximum value reported for the uncarbonated mix (10.12 MPa and 10.68 MPa respectively). It can be concluded that the highest relative increase in flexural

strength due to carbonation occurs for the mixes with the highest proportions of MIBA, as it is a precursor with relatively high calcium content.
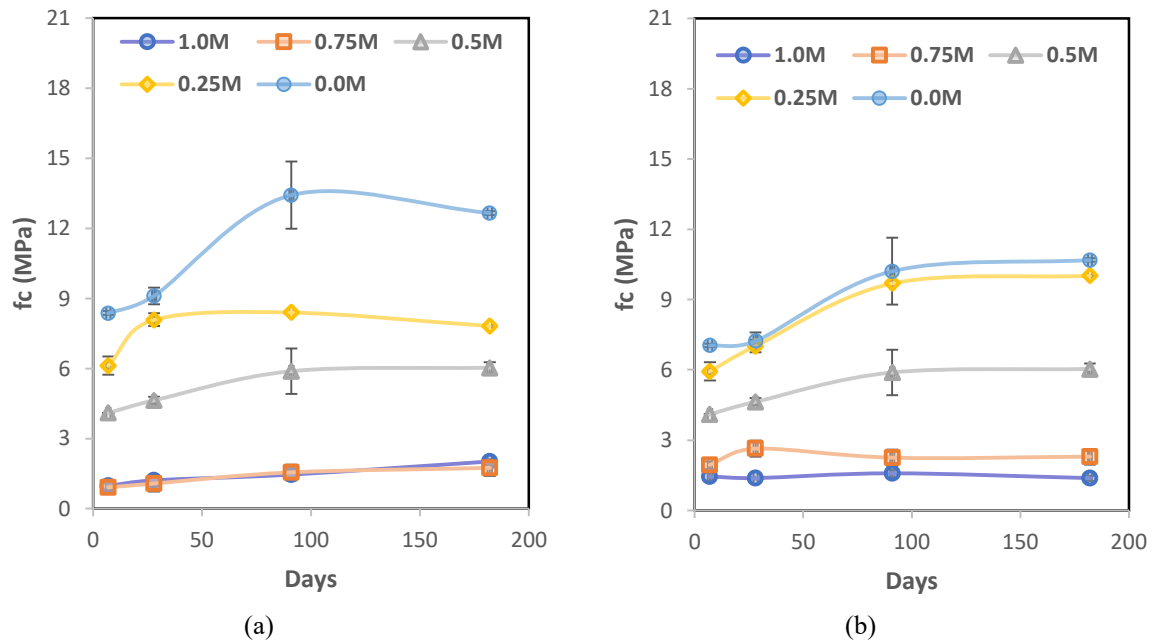

Figure 14 - Flexural strength of: (a) OAA mortars and (b) CAA mortars
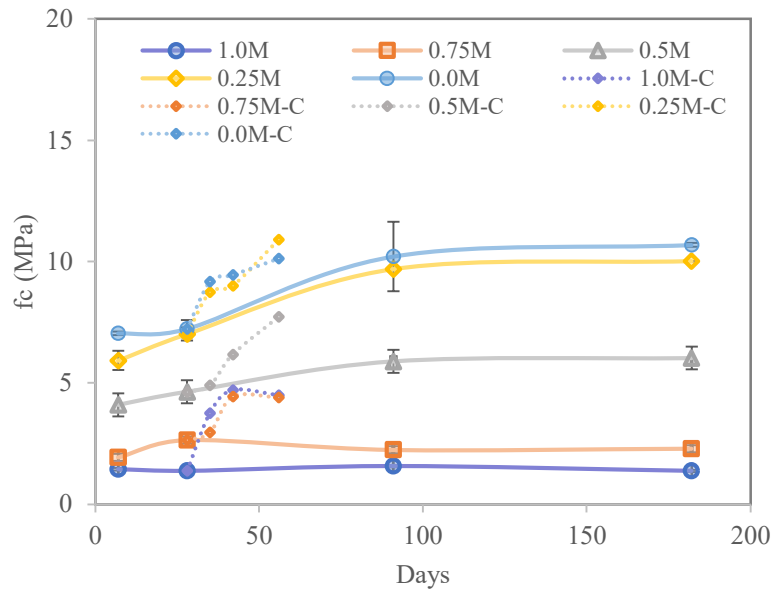
Figure 15 - Variation in flexural strength values between uncarbonated and carbonated mortars with CAA design

3.4.3   Dynamic modulus of elasticity

Figure 16 shows the results of the dynamic modulus of elasticity at 7, 28, 91 and 182 days for the mortars made with the OAA and the CAA designs. The maximum dynamic modulus of elasticity obtained for each alkaline activator design at 28 days corresponds to the mix with 100% FA: 28.1 GPa and 24.9 GPa for the OAA and CAA designs, respectively. The minimum values correspond to the mix with 75% MIBA (i.e. 4.96 GPa) for the OAA design and 100% MIBA (i.e. 4.44 GPa) for the CAA design. For longer curing times, the trend is maintained with respect to mixes with the highest and lowest modulus dynamic of elasticity.

Dynamic modulus of elasticity presented higher values with the OAA design when the FA content was greater than 50%, but if the replacement was less than this percentage, the results were better with the CAA design. For both designs, the dynamic modulus of elasticity increased with increasing FA content in the mix, and more so when going from 25% to 50% FA (around 62%).

<table>
<tr><td>(a)</td><td>(b)</td></tr>
</table>

Figure 16 - Dynamic modulus of elasticity of: (a) OAA mortars and (b) CAA mortars

The dynamic modulus of elasticity is directly influenced by the porosity/density, cohesion of particles and the presence of microcracks in the hardened material. Given the characteristics of MIBA as a precursor, it was expected that prismatic specimens with a higher content of this

precursor would present a lower dynamic modulus of elasticity. The opposite occurred for the mixes that contained a greater amount of FA (0.25M and 0.0M). These AAM presented a dynamic modu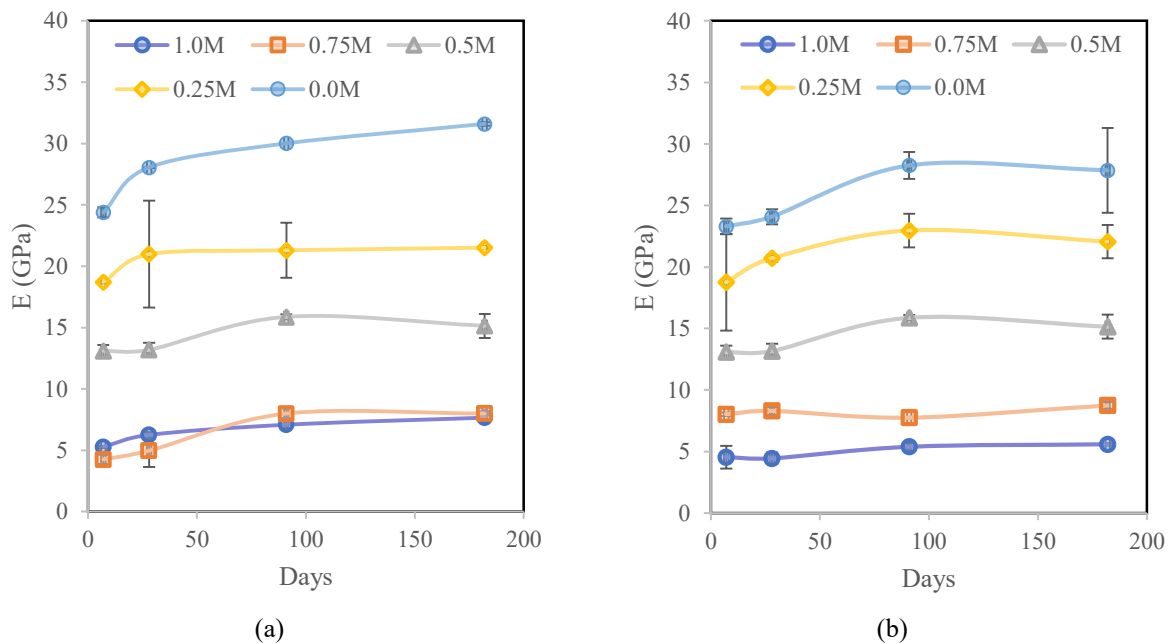lus of elasticity greater than 20 GPa after 28 days. This result is in accordance with that reported by Fernandez-Jimenez et al. [41], who obtained an average value of 17.1 GPa for the dynamic modulus of elasticity at 28 days for alkali-activated concrete with FA as precursor and a mix of NaOH and Na_2SiO_3 as alkaline activator.

Figure 17 shows the linear correlation between the modulus of elasticity and the compressive strength for the OAA design (Figure 17a) and the CAA design (Figure 17b) mixes. The R^2 obtained corresponds to 0.98 and 0.97 respectively, showing that there is a linear relationship between these two properties.

| (a) | (b) |
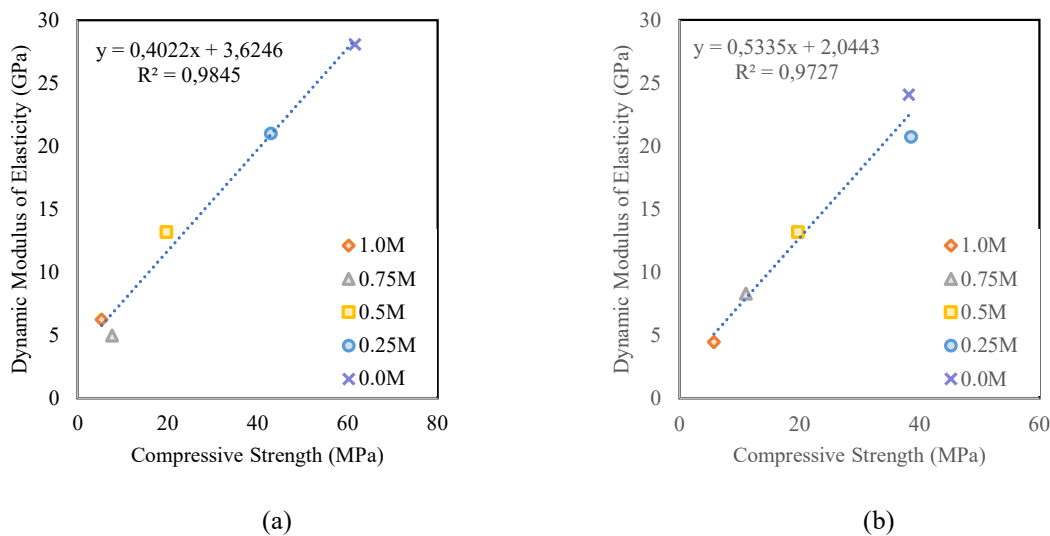
Figure 17 - Correlation between the dynamic modulus of elasticity and compressive strength for: (a) OAA mortars and (b) CAA mortars

3.4.4 Shrinkage

Figure 18 shows the shrinkage results for the mortars with CAA design. Measurements were made on sealed and unsealed mortars, in order to evaluate the shrinkage variation under these conditions. Shrinkage in both cases (sealed and unsealed) increased with increasing MIBA content. The highest shrinkage at 115 days occurred in mortars made with 100% MIBA (1600 µm/m and 1300 µm/m, respectively). In both figures, it can be observed that the mixes with MIBA contents greater than 50% present curves very close to each other, while the mixes with

75% or 100% FA have a different behaviour, constituting another group.

(a)   (b)
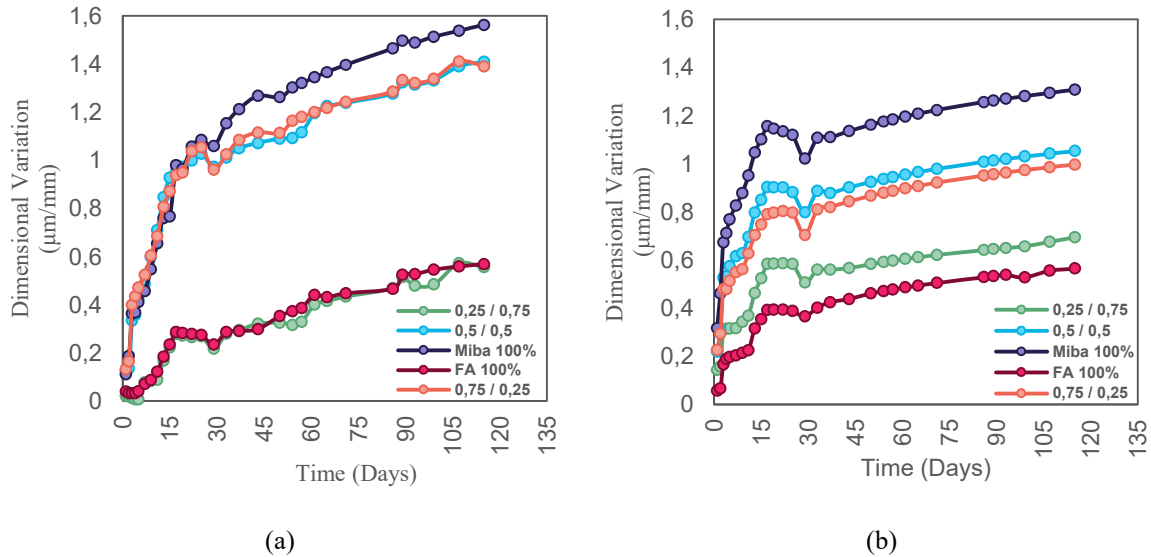
Figure 18 - Shrinkage of the mortars with CAA design and (a) sealed or (b) unsealed curing

Carvalho et al. [42] reported in their research that MIBA presents a morphology of irregular particles and porous microstructure. According to Kuenzel et al. [43], shrinkage is directly influenced by the interconnected porosity of the material, so it could be inferred that, for MIBA percentages greater than 50%, the pre-treatment was not satisfactory, resulting in a remnant of unreacted metallic aluminium, which led to damaging foaming reactions when in contact with Na_2SiO_3, increasing the porosity of the mortar in the hardened state. Moreover, all mortars were exposed to thermal curing for 24 hours, which accelerates water evaporation during the setting stage. This rapid water loss could have led to the formation of microcracks in the specimens [44].

The shrinkage of sealed specimens made with cement is usually lower than that of unsealed ones, due to the greater water loss of the latter. In this case, the opposite was observed and most likely due to the existence of the thermal curing stage, which significantly reduced the water content of the specimens. Sealed specimens, which have minimal exchange of water with the environment, exhibited shrinkage associated with the internal reactions within the AAM matrix, where a major consumption of internal water occurred. On the other hand, unsealed mortar specimens, after their thermal activation and throughout the curing process, were in a ~60% RH environment. This allowed gas exchange, favouring especially the increase in

humidity of the specimens towards an equilibrium in the water vapour concentration with that of the external environment. Naturally, this led to a hydration of the AAM matrix, offsetting the shrinkage caused by the internal reactions.

Yang et al. [45] studied the autogenous shrinkage of alkali-activated materials sealed with a polyethylene film, concluding that storage conditions influence shrinkage. However, in the case of AAMs, autogenous shrinkage cannot be explained by the same theory as that of cement self-shrinkage, since there is a direct dependence between shrinkage and relative humidity [46].

3.4.5 Water absorption by capillary action

The water absorption by capillary action test was carried out solely on the mixes with CAA design in order to eliminate the influence of the SiO_2/Na_2O and Na_2O/binder variables. Figure 19 shows the results of capillary absorption coefficients in $kg/(m^2.min^{0.5})$ for each mix. Figure 19a corresponds to the coefficients obtained for the first stage of the test (measurements between 10 and 90 minutes), while Figure 19b corresponds to the coefficients calculated for the second stage of the test (measurements between 90 and 4320 minutes).

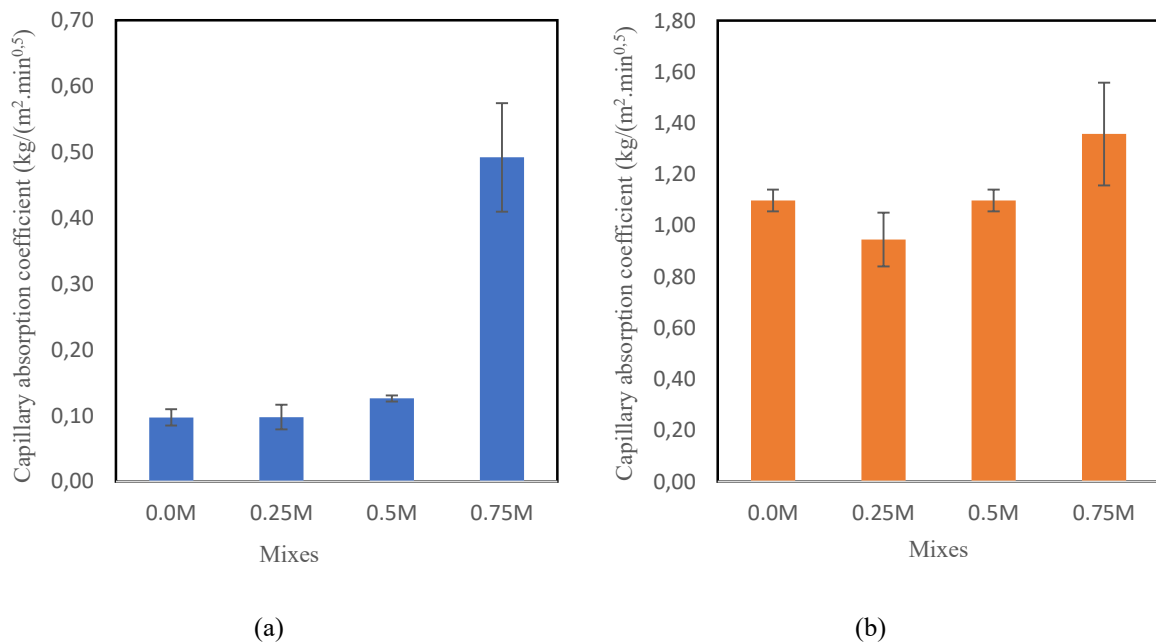(a)   (b)

Figure 19 - Capillary absorption coefficients of CAA mortars: (a) between 10 and 90 minutes and (b) between 90 and 4320 minutes

Figure 19b shows that the capillary coefficient was similar for mixes with MIBA contents equal to and below 50%, increasing remarkably for higher MIBA contents. The results are somewhat in accordance with the previous ones for other properties, again suggesting that the mortars with greater amounts of MIBA are more porous and, therefore, more susceptible to water movement. It should be noted that the capillarity coefficients obtained for 1.0M mortars are not shown, since these mortars presented considerable mass loss during the test (Figure 20).

(a)   (b)

Figure 20 - Capillarity test: (a) experimental setup and (b) 1.0M mortar with loss of mass after 90 minutes

Researchers on the matter have expressed different points of view regarding the role of alkali (in the present work it corresponds to Na^+) in the chemical structure of the oligomers formed. According to Davidovits [47], the poor physicochemical properties of some AAM are associated with the fact that the Na^+ ion is located at the boarders of the cyclic oligomers, which means that it easily migrates to the surface in contact with it (i.e. water). According to this author, the opposite occurs when the chemical structure formed is a three-dimensional network where the Na^+ ion is fixed and trapped within the framework. On the other hand, there are authors such as Ben Haha et al. [48], San Nicolas et al. [49] or Bernal et al [50], whose studies reveal that some chemical bridges of Ca^{2+} in C-A-S-H are replaced with Na^+, giving rise to C-(N)-A-S-H when using precursors such as blast furnace slag, which has a high Ca^{2+} content.

The results of the capillarity test indicate that, for the precursor rich in Ca^{2+} (i.e. MIBA) and the precursor low in Ca^{2+} (i.e. FA), Na^+ dissolves and leaches out of the mortars when water enters the capillaries, which indicates that a given amount of alkali is not physically bound

within the matrix. This phenomenon was more noticeable in the specimens with a higher MIBA content, where the migration of excess Na^+ towards the surface gives rise to the precipitation of products (e.g. efflorescence of sodium carbonate).

3.4.6 Water absorption by immersion

Table 4 shows the results of the water absorption by immersion. Similar to the mechanical and durability properties, the percentage of water absorption increases with increasing MIBA content, despite presenting a similar value for the mixtures 0.0M and 0.25M. It was not possible to obtain results for the 0.75M and 1.0M mixes, since the specimens broke 24 hours after being submerged due to excessive loss of mass (Figure 21). This result confirms what was mentioned in section 3.4.1, associated with the hydration products formed from the mixes, as well as the low content of amorphous phases present in the MIBA precursor.

Table 4 - Water absorption by immersion of the mortars with CAA design

Mix	Water absorption by immersion (%)	Standard deviation
0.0M	13.4	0.14
0.25M	13.1	0.09
0.5M	14.8	0.30

(a)   (b)

Figure 21 - CAA mortars 24 h after immersion in water: (a) 75% MIBA and (b) 100% MIBA

4 Conclusions

From the previous results, it is possible to conclude that:

- The chemical and mineralogical characterization of MIBA showed that it has potential to be activated, but the high aluminium content is problematic in alkali-activated materials due to the formation of hydrogen gas;
- The pre-treatment was effective at reducing the amount of pure aluminium available to react, thereby allowing the production of mortars with adequate dimensional stability;
- FA improved the workability of the mixes in the fresh state, regardless of the activator design. Still, the mixes with CAA design presented a higher fluidity since they had the lowest sodium silicate content;
- MIBA led to a less dense material (due to the foaming reaction between the residual aluminium with the alkaline activator), a higher porosity, lower mechanical strength and higher water absorption, especially in contents equal to or greater than 75%. However, mixes with a maximum of 50% MIBA content did not show an excessive deterioration in the mechanical properties and durability evaluated;
- Carbonation improved substantially the mechanical properties of AAM, especially in those with higher contents of MIBA, as it is a precursor with a high calcium content;
- Shrinkage of the sealed and unsealed specimens is influenced by thermal curing and storage conditions; therefore, the sealed specimens exhibited higher shrinkage;
- All mixes presented sodium migration when performing the capillary test, the magnitude of which was greater in mixes with a greater amount of MIBA, concluding that this element is not trapped in the structure of the gel formed.

Acknowledgements

References

1. Eurostad statistic xplained, Municipal Waste Statistic. 2019 [Access date: 07 July 2021].

2. Zhang, Y., et al., Treatment of municipal solid waste incineration fly ash: State-of-the-art technologies and future perspectives. Journal of Hazardous Materials, 2021. 411: p. 125132.

3. EN 1015-3, European Standard, Methods of test for mortar for masonry - Part 3: Determination of consistence of fresh mortar (by flow table), European Committee for Standardization (CEN), 1999, Brussels, Belgium.

4. EN 1015-6, European Standard, Methods of test for mortar for masonry - Part 6: Determination of bulk density of fresh mortar, European Committee for Standardization (CEN), 1998, Brussels, Belgium.

5. EN 1015-11, European Standard, Methods of test for mortar for masonry - Part 11: Determination of flexural and compressive strength of hardened mortar, European Committee for Standardization (CEN), 1999, Brussels, Belgium.

6. EN 1015-10, European Standard, Methods of test for mortar for masonry - Part 10: Determination of dry bulk density of hardened mortar, European Committee for Standardization (CEN), 1999, Brussels, Belgium.

7. ASTM-E1876, Standard Test Method for Dynamic Young's Modulus, Shear Modulus, and Poisson's Ratio by Impulse Excitation of Vibration, American Society for Testing and Materials, 2015, West Conshohocken, Pennsylvania, USA.

8. EN-1015-13, European Standard, Methods of test for mortar for masonry - Part 13: Methods of test for mortar for masonry - Part 13: Determination of dimensional stability of hardened mortars, European Committee for Standardization (CEN), 1993, Brussels, Belgium.

9. BS EN 1015-18 European Standard, Natural stone test methods. .Determination of water absorption coefficient due to capillary action of hardened mortar, European Committee for Standardization (CEN), 2002: Brussels, Belgium.

10. LNEC- E394, Concrete: determination of water absorption by immersion - testing at atmospheric pressure (in Portuguese), 1993. National Laboratory in Civil Engineering (LNEC - Laboratório Nacional de Engenharia Civil) Lisbon, Portugal.

11. LNEC- E391, Concrete: Determination of carbonation resistance, (in Portuguese), 1993, National Laboratory in Civil Engineering (LNEC - Laboratório Nacional de Engenharia Civil) Lisbon, Portugal.

12. Duxson, P., et al., Geopolymer technology: the current state of the art. Journal of materials science, 2007. 42(9): pp. 2917-2933.

13. ASTM C618, Standard Specification for Coal Fly Ash and Raw or Calcined Natural Pozzolan for Use in Concrete, American Society for Testing and Materials 2019, West Conshohocken, Pennsylvania, USA.

14. Lynn, C.J., R.K. Dhir, and G.S. Ghataora, Municipal incinerated bottom ash use as a cement component in concrete. Magazine of Concrete Research, 2017. 69(10): p. 512-525.

15. Lothenbach, B., K. Scrivener, and R. Hooton, Supplementary cementitious materials. Cement and concrete research, 2011. 41(12): pp. 1244-1256.

16. Cristelo, N., et al., Recycling municipal solid waste incineration slag and fly ash as precursors in low-range alkaline cements. Waste Management, 2020. 104: pp. 60-73.

17. Huang, G., et al., Influence of NaOH content on the alkali conversion mechanism in MSWI bottom ash alkali-activated mortars. Construction and Building Materials, 2020. 248: p. 118582.

18. Wei, Y., et al., Geoenvironmental weathering/deterioration of landfilled MSWI-BA glass. Journal of Hazardous Materials, 2014. 278: p. 610-619.

19. Bayuseno, A.P. and W.W. Schmahl, Understanding the chemical and mineralogical properties of the inorganic portion of MSWI bottom ash. Waste Management, 2010. 30(8-9): pp. 1509-1520.

20. Cho, Y.K., et al., Effect of Na2O content, SiO2/Na2O molar ratio, and curing conditions on the compressive strength of FA-based geopolymer. Construction and Building Materials, 2017. 145: pp. 253-260.

21. Rashad, A.M. and S.R. Zeedan, The effect of activator concentration on the residual strength of alkali-activated fly ash pastes subjected to thermal load. Construction and Building Materials, 2011. 25(7): pp. 3098-3107.

22. ASTM D4972, Standard Test Methods for pH of Soils, American Society for Testing and Materials 2019, West Conshohocken, Pennsylvania, USA.

23. Engineering ToolBox. Hydrogen - Density and specific weight. 2018: https://www.engineeringtoolbox.com/hydrogen-H2-density-specific-weight-temperature-pressure-d_2044.html

24. NBR 15895. Materiais pozolânicos - Determinação do teor de hidróxido de cálcio fixado – Método Chapelle modificado, Brazilian Association for Technical Norms (Associação Brasileira de Normas Técnicas-ABNT) Rio de Janeiro,Brasil, 2010.

25. Raverdy, M., et al., Appréciation de l'activité pouzzolanique de constituents secondaires. Proceedings of 7e congrés international de la chimie des ciments, Paris, France, 1980: pp. 6-41.

26. Hoppe Filho, J., Atividade pozolânica de adições minerais para cimento Portland (Parte I): Índice de atividade pozolânica (IAP) com cal, difração de raios-X (DRX), termogravimetria (TG/DTG) e Chapelle modificado. Revista Matéria, 2017. 22(3).

27. Kuenzel, C. and N. Ranjbar, Dissolution mechanism of fly ash to quantify the reactive aluminosilicates in geopolymerisation. Resources, Conservation and Recycling, 2019. 150: p. 104421.

28. Liu, Y., et al., Alkali-treated incineration bottom ash as supplementary cementitious materials. Construction and Building Materials, 2018. 179: pp. 371-378.

29. Mary Joseph, A., et al., Pre-treatment and utilisation of municipal solid waste incineration bottom ashes towards a circular economy. Construction and Building Materials, 2020. 260: p. 120485.

30. Rosenband, V. and A. Gany, Application of activated aluminum powder for generation of hydrogen from water. International Journal of Hydrogen Energy, 2010. 35(20): pp. 10898-10904.

31. Das, S.K., et al., Fresh, strength and microstructure properties of geopolymer concrete incorporating lime and silica fume as replacement of fly ash. Journal of Building Engineering, 2020. 32: p. 101780.

32. Kuri, J.C., M.N.N. Khan, and P.K. Sarker, Fresh and hardened properties of geopolymer binder using ground high magnesium ferronickel slag with fly ash. Construction and Building Materials, 2021. 272: p. 121877.

33. Provis, J.L., P. Duxson, and J.S. van Deventer, The role of particle technology in developing sustainable construction materials. Advanced Powder Technology, 2010. 21(1): pp. 2-7.

34. Eliche-Quesada, D., et al., Dust filter of secondary aluminium industry as raw material of geopolymer foams. Journal of Building Engineering, 2020: p. 101656.

35. Provis, J.L., et al., Binder chemistry–Low-calcium alkali-activated materials, in Alkali Activated Materials. 2014, Springer. pp. 93-123.

36. Bernal, S.A., et al., Binder chemistry–high-calcium alkali-activated materials, in Alkali activated materials. 2014, Springer. pp. 59-91.

37. Wongsa, A., et al., Use of municipal solid waste incinerator (MSWI) bottom ash in high calcium fly ash geopolymer matrix. Journal of Cleaner Production, 2017. 148: pp. 49-59.

38. Hosseini, S., et al., Mechanochemically activated bottom ash-fly ash geopolymer. Cement and Concrete Composites, 2021. 118: p. 103976.

39. Casanova, S., et al., Mortars with alkali-activated municipal solid waste incinerator bottom ash and fine recycled aggregates. Journal of Cleaner Production, 2021. 289: p. 125707.

40. Huang, G., et al., Use of slaked lime and Portland cement to improve the resistance of MSWI bottom ash-GBFS geopolymer concrete against carbonation. Construction and Building Materials, 2018. 166: pp. 290-300.

41. Fernandez-Jimenez, A.M., A. Palomo, and C. Lopez-Hombrados, Engineering properties of alkali-activated fly ash concrete. ACI Materials Journal, 2006. 103(2): p. 106.

42. Carvalho, R., et al., Alkali activation of bottom ash from municipal solid waste incineration: Optimization of NaOH- and Na 2SiO3-based activators. Journal of Cleaner Production, 2021. 291: p. 125930.

43. Kuenzel, C., et al., Ambient temperature drying shrinkage and cracking in metakaolin-based geopolymers. Journal of the American Ceramic Society, 2012. 95(10): pp. 3270-3277.

44. Tian, Q., et al., Alkali-activated materials as coatings deposited on various substrates: A review. International Journal of Adhesion and Adhesives, 2021. 110: p. 102934.

45. Yang, T., H. Zhu, and Z. Zhang, Influence of fly ash on the pore structure and shrinkage characteristics of metakaolin-based geopolymer pastes and mortars. Construction and Building Materials, 2017. 153: pp. 284-293.

46. Archez, J., et al., Influence of the geopolymer formulation on the endogeneous shrinkage. Construction and Building Materials, 2021. 298: p. 123813.

47. Davidovits, J., Geopolymer chemistry and applications. 2008: Geopolymer Institute.

48. Haha, M.B., et al., Influence of activator type on hydration kinetics, hydrate assemblage and microstructural development of alkali activated blast-furnace slags. Cement and Concrete Research, 2011. 41(3): pp. 301-310.

49. San Nicolas, R. and J. Provis. Interfacial transition zone in alkali-activated slag concrete. in Proceedings of the 12th International Conference on Recent Advances in Concrete Technology and Sustainability Issues, Prague, Czech Republic. 2012.

50. Bernal, S.A., et al., Natural carbonation of aged alkali-activated slag concretes. Materials and structures, 2014. 47(4): pp. 693-707.

Authors

Yoleimy Ávila Pereira	Bruna A. Silva
PhD Candidate	PhD Researcher
Rui Vasco Silva	Jorge de Brito
PhD Researcher	Full Professor